Expansion and cooling of a bright rubidium three-dimensional optical molasses

Laurence Pruvost,* Isabelle Serre, Hong Tuan Duong, and Joshua Jortner†
Laboratoire Aimé Cotton, CNRS II, Batiment 505, Campus d'Orsay, 91405 Orsay, France
(Received 28 September 1999; published 14 April 2000)

We have studied the expansion of a bright rubidium three-dimensional optical molasses realized with an intense laser light. In this regime, in addition to the laser friction force, the atoms strongly repel each other due to the radiation trapping force, which is analogous to the Coulomb force. The experimental observations show that the cloud volume increases linearly in time and that, simultaneously, the cloud temperature decreases following the law $(1+t/\tau)^{-4/3}$. These time evolutions are explained using a physical picture of Coulomb explosion in a viscous medium.

PACS number(s): 32.80.Pj

I. INTRODUCTION

For many years, laser cooling and laser trapping have been extensively studied, with various geometry configurations, with various laser polarizations, and with many atoms. In usual optical traps, the momentum exchange between the laser light and the atom leads to a friction force, which reduces the atom velocity and cools it down. In a magneto-optical trap (MOT), the confinement is done because of the presence of a magnetic field gradient which, combining to the light, induces a restoring force towards the zero-magnetic field region. These two forces are the main ingredients to understand the behavior of the atoms in MOT realized with laser at a low saturation parameter.

For large cloud densities, and, for intense trapping laser (large saturation parameter), these ingredients are not enough to explain the cloud properties and behavior. Some other processes have to be taken into account to describe correctly the properties of the atomic cloud, i.e., the absorption of the laser light by the cloud and the multiple scattering of photons in the cloud. The absorption of light induces a laser intensity gradient and therefore modifies the radiation pressure force [1]. The so-called absorption force is larger at the cloud border than at its center. Therefore, the absorption force compresses the cloud. The multiple scattering of photons in the atomic cloud induces the radiation trapping force [2]. As explained by Sesko, Walker and Wieman [3], the photons emitted by an atom can be reabsorbed by a neighboring atom and this photon exchange leads to a repulsive force between the atoms. The radiation trapping force is proportional to the reabsorption cross section, which depends not only on the emission spectra but also on the absorption of the neighbor. In the presence of an intense laser light, the emission and the absorption spectra are modified. The emission spectrum exhibits a structure with three components (the Mollow triplet) [4,5]. The blue component contains photons nearly at resonance, which can be efficiently absorbed, because the absorption spectrum [6] is asymmetric with its main component blue shifted. Consequently, the reabsorption cross-section is enhanced and also the radiation trapping force. In the weak-intensity regime, the radiation trapping force balances the absorption force and becomes larger in the multiple scattering regime.

In a MOT, many experimental manifestations are due to the absorption and to radiation trapping forces. For bright optical traps and for clouds with a large atom number, these forces are responsible for the limitation of the atomic density and for the cloud shape [7–9]. In the case of slightly misaligned laser beams, the forces explain the spatial structures observed in the atomic cloud [10]. In MOT and in optical molasses (OM), the fluctuations of these forces explain the observed temperatures and the limitation for lower temperatures in dense atomic clouds [9,11].

In this paper we analyze the manifestations of absorption and radiation trapping forces by another way. We realize a dynamical study of a bright OM. We first fill a MOT. Subsequently, we suppress the restoring force. Therefore, we get an OM, which expands only under the absorption and radiation trapping forces and the friction force. The laser light being intense, the effects of the absorption and radiation trapping forces dominate and contrary to previous studies [12,13], the atom momentum diffusion due to the photon exchange with the cooling laser becomes negligible. During the cloud expansion, we record the atom number, the size, the shape, and the temperature. The absorption and radiation trapping forces decrease as the cloud expands, whereupon we observe a decrease of the temperature simultaneously with the expansion. The observed expansion and the cooling are reproduced and explained using a Coulomb explosion model in a viscous medium.

As explained in Ref. [3] the radiation trapping force between two atoms is proportional to $1/r_{12}^2$, where r_{12} is the distance between the atoms. The radiation trapping force is analogous to the Coulomb law and the expansion of the cloud can be viewed as a Coulomb explosion. To obtain a correct order of magnitude estimate for the radiation trapping force, the effective charge to put in the Coulomb law is about $10^{-5}e$, where e is the electron charge ($e=1.6\times10^{-19}$ C). According to Coulomb explosion models, usually used for charged molecules and clusters [14–15], the Coulomb explo-

*Author to whom all correspondence should be addressed. Present address: Laboratoire Aimé Cotton, CNRS II, Batiment 505, Campus d'Orsay, 91405 Orsay. FAX: 01 69 35 21 00. Electronic address: pruvost@sun.lac.u-psud.fr

†Permanent address: School of Chemistry, Tel Aviv University, Ramat Aviv, 69978 Tel Aviv, Israel.

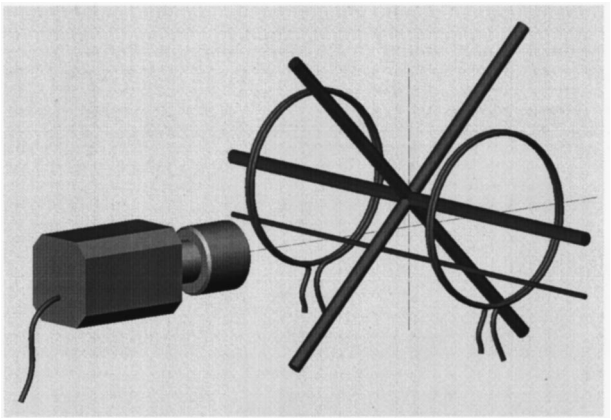

FIG. 1. Experimental scheme. The three laser beams cross at the center of the anti-Helmoltz coils. The horizontal probe beam is located 1 cm below the center of the trap. The cloud, and the fluorescence in the probe beam are imaged onto the CCD camera.

sion time is $\tau_c \propto q^{-1} m^{1/2} R_0^{3/2}$, where q is the constituent charge, m its mass and R_0 the initial interparticle spacing. The OM is characterized by a small charge $q \cong 10^{-5} e$ and by large values (on the microscopic scale) of $R_0 \sim 10^{-4}$ cm, corresponding to typical densities of 10^{11} atoms/cm^3. Accordingly, the Coulomb explosion time scales by a numerical factor of 10^{10} from 100 fs in large molecules and clusters of heavy atoms, e.g., Xe [14–15], to ~1 ms in the bright OM of Rb. In an OM, in addition to the Coulomb force, the atoms are submitted to the friction force due to the laser. The expansion of a bright OM is thus analogous to a Coulomb explosion in a viscous medium. The viscosity increases the time scale of the expansion. We benefit of this advantage to perform an experimental analysis of the cloud expansion, using an imaging method. Note also that the bright OM constitutes a simple experimental system for the interrogation of Coulomb explosion. In clusters and molecules, other phenomena are often in competition with the Coulomb explosion, for example, the fission, dissociation, or evaporation. In plasmas, the presence of positive and negative charges changes considerably the dynamics of the temporal evolution. In our study, we have no competitive processes and the Coulomb explosion parameters can be modified by the variation of laser parameters (intensity and frequency).

The presentation of the paper is the following. Section II is devoted to the experimental setup. We give the procedure for recording the cloud images and for analyzing the temperature versus time. In Sec. III, we present experimental results for the cloud expansion, the model for the Coulomb explosion of a viscous medium and a comparison with the experimental data. In Sec. IV, we present the cooling of the expanding cloud and we compare the experimental temperature to the model. Section V summaries our conclusions.

II. THE EXPERIMENT

A schematic view of the experimental setup is given in Fig. 1. The MOT is realized at the center of a non-magnetic stainless steel vacuum chamber evacuated by a 20 1/s ionic pump (Varian, 20 1/s). The achieved vacuum is about 10^{-9} Torr, measured by monitoring the ionic pump current. At the center of the chamber, in a volume of 8 cm^3, the magnetic fields are reduced to zero (less than 1 mG $= 10^{-7}$ T), by using three pairs of Helmholtz coils.

The MOT magnetic-field gradient is produced at the center of the chamber by a pair of water cooled anti-Helmholtz coils with a magnetic gradient, b_x, along the coil axis, up to 25 gauss/cm. The MOT is realized by 3 retroreflected $\sigma^+ - \sigma^-$-polarized laser beams in three orthogonal space directions. The laser beams are provided by laser diodes, which frequencies are locked to cross-over lines of the saturated absorption spectrum of the $5S_{1/2} \rightarrow 5P_{3/2}$ ^{85}Rb transition. The cooling laser beam is provided by a 50 mW, Hitachi diode laser, 10 MHz line width, which frequency is locked to a cross-over resonance located at 92 MHz from the $5S_{1/2}$ $F = 3 \rightarrow 5P_{3/2}$ $F' = 4$ cooling transition. The cooling laser frequency detuning, δ, measured relatively to the atomic resonance, is then tuned in the range $-1.5\,\Gamma$ to $-7\,\Gamma$, where Γ is the natural width of the cooling transition ($\Gamma = 2\pi$ 5.89 MHZ). This frequency detuning is accomplished via an acousto-optic modulator of a central frequency of 80 MHz. The laser beam is made round by using anamorphic prisms, and expanded to a 0.36 cm^2 size (the $1/e^2$ radius being equal to 3.4 mm). At the entrance of the vacuum chamber up to 12 mW laser power is available. It allows to vary the ratio I/I_s up to 20 (I is the six-beam total intensity and I_s is the saturation intensity, equal to 1.62 mW/cm^2 for $5S_{1/2}$ $F = 3$ $M = 3 \rightarrow 5P_{3/2}$ $F' = 4$ $M' = 4$ of the Rb atom). Another laser diode provides the repumping beam. Its frequency is stabilized to the $5S_{1/2}$ $F = 2 \rightarrow 5P_{3/2}$ $F' = 2$ transition. About 5 mW of power is used. This beam overlaps the cooling laser beam in the three directions of space.

To produce the OM, switching on the magnetic field gradient and the lasers, we first fill the MOT for 4 s, which is longer than the trap filling time constant (2 s). The OM is obtained by rapidly switching off the magnetic field gradient, the laser parameters (intensity, frequency and polarization) remaining the same. The measured switching time of the anti-Helmholtz coil current is less than 500 μs. Some residual eddy currents limit the magnetic-field gradient switching time to 1 ms. The OM submitted to the already mentioned forces rapidly expands. At time t the lasers are switched off via the acousto-optics devices. A mechanical shutter is added to eliminate any residual light.

Just before switching off the lasers, the cloud image is formed onto a charge coupled device (CCD) camera. The CCD exposure is started by opening the shutter located in front of the detector and by triggering the camera electronics. The cloud fluorescence is collected by a 6-cm focal length anti reflection coated doublet lens with effective aperture 2.8 cm. The camera device is a commercial (Princeton Instrument) nitrogen cooled camera. Its CCD array contains 512 $\times$512, 24$\times$24 μm size, pixels with 70% quantum efficiency. Stray ambient light is reduced by using an interferometric filter, with a 83% transmission at 780 nm. To avoid any CCD array saturation, the detector exposure begins just before the trapping laser beams are switched off. We obtain a cloud exposure corresponding to a cloud emission time of 1 ms.

When the lasers are off, the cloud falls down. A probe laser beam located 6 mm below the center of the trap is used to image the fluorescence of the cloud as it falls across. The probe beam is 2 mm diameter sized, -3Γ red detuned from resonance, by using another acousto-optic device. The beam is retro-reflected with orthogonal linear polarization (linear $\perp$ linear configuration), in order to get a molasses effect in the detection. This detection configuration avoids any atom displacement in the probe beam due to radiation pressure force, and allows a long interaction time in the probe beam. A weak repumping beam (0.1 mW), provided by the above mentioned laser is superimposed on this beam. The probe beam light is switched on during 10 ms, when the atom packet is passing through. The detector exposure time is chosen to be long enough, in order to obtain the OM image and the cloud fluorescence in the probe beam with the same CCD record. Such a record is shown in Fig. 2. To study the dynamics of the cloud expansion we record such an exposure for different values of the expansion time t.

The top region of each exposure is numerically integrated and gives the total number of counts, which is proportional to the OM atom number. For this measurement we assume a two level atom model for the calculation of the fluorescence rate. We do not take into account the beam polarization and the cloud position in the intersection of the light beams. Therefore the absolute atom number uncertainty is about 30%, but the cloud atom number variations are quantitatively analyzed. The OM image is numerically integrated over rows and over columns and gives the horizontal [Fig. 2(b)] and vertical cloud profiles. The cloud profiles are well fitted by gaussian profiles giving the $1/e^2$ cloud radii, σ_x along the x axis corresponding to the magnetic field gradient b_x and σ_z in the vertical direction. The OM size is measured with a precision of 28 μm.

The bottom region of each exposure is numerically integrated over 10 rows. The obtained profile is plotted in Fig. 2(c). Its width, σ_t, depends on the atomic velocity distribution in the OM at the time t. If the position and velocity distributions are not correlated, σ_t depends only on the OM size, σ_0, its temperature, T, and the time of flight, t_f, by the relation $\sigma_t^2=\sigma_0^2+aTt_f^2$, where a is a constant. If the position and the velocity distributions are correlated this relation is no longer valid. In our experiment, the radiation trapping force induces a strong correlation between velocity and position and the measurement of the cloud ''temperature'' requires some assumptions. Assuming the correlation described in Secs. II and IV, σ_t is related to σ_0 by the relation $\sigma_t=\sigma_0+\nu_m t_f$, where ν_m is the mean radial velocity.

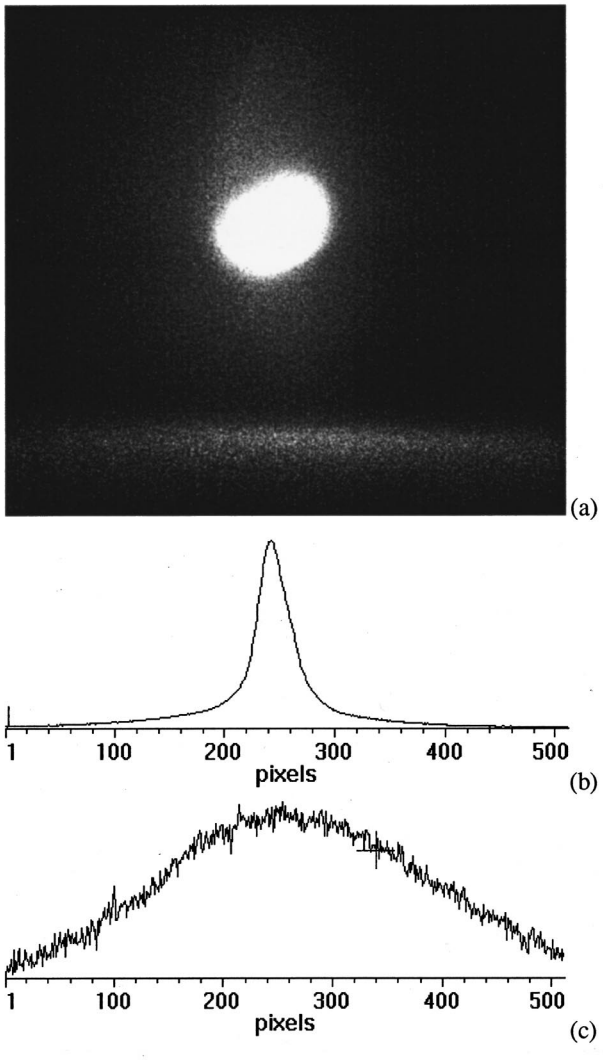

FIG. 2. Exposure of the molasses and its fluorescence in the probe beam. (a) The exposure for $\delta/\Gamma=-3.7$, $I/I_s=20$, obtained at $t=20$ ms. (b) The molasses profile along the x axis, (220 line integration) used to deduce the cloud dimension. (c) Fluorescence in the probe beam (100 line integration) used to deduced the cloud temperature.

III. EXPANSION OF THE BRIGHT MOLASSES

A. Experimental results

The time evolution of the OM has been recorded for a laser intensity in the range of $I/Is=15-20$ and for a set of laser detuning ($\delta/\Gamma=-1.5,-2.5,-3.7,-5.4,-6.8$). Figure 3 shows the experimental data for $I/I_s=17.5$ and $\delta/\Gamma=-3.7$.

We observe an exponential decrease of the atom number [Fig. 3(a)] with a time constant of $\sim$400 ms, which is large compared to the evolution time of the cloud size [Fig. 3(b)]. For the time range of our interest (up to 200 ms) we can thus consider that the atom number remains nearly constant during the cloud expansion.

The cloud expansion [Fig. 3(b)] is fast. The cloud size reaches twice its initial value on a time scale of about some milliseconds. The observation does not correspond to a momentum diffusion process, which is expected to occur on the time scale of seconds [12]. The millisecond time scale is in agreement with the scaling argument for the Coulomb explosion, as already mentioned in Sec. I.

According to Fig. 3(c), we observe a linear time dependence of the cloud volume. Consequently the mean cloud density rapidly decreases as shown in Fig. 3(d). Again, the observations rule out the momentum diffusion process, where the square of the cloud size evolves linearly with time [12].

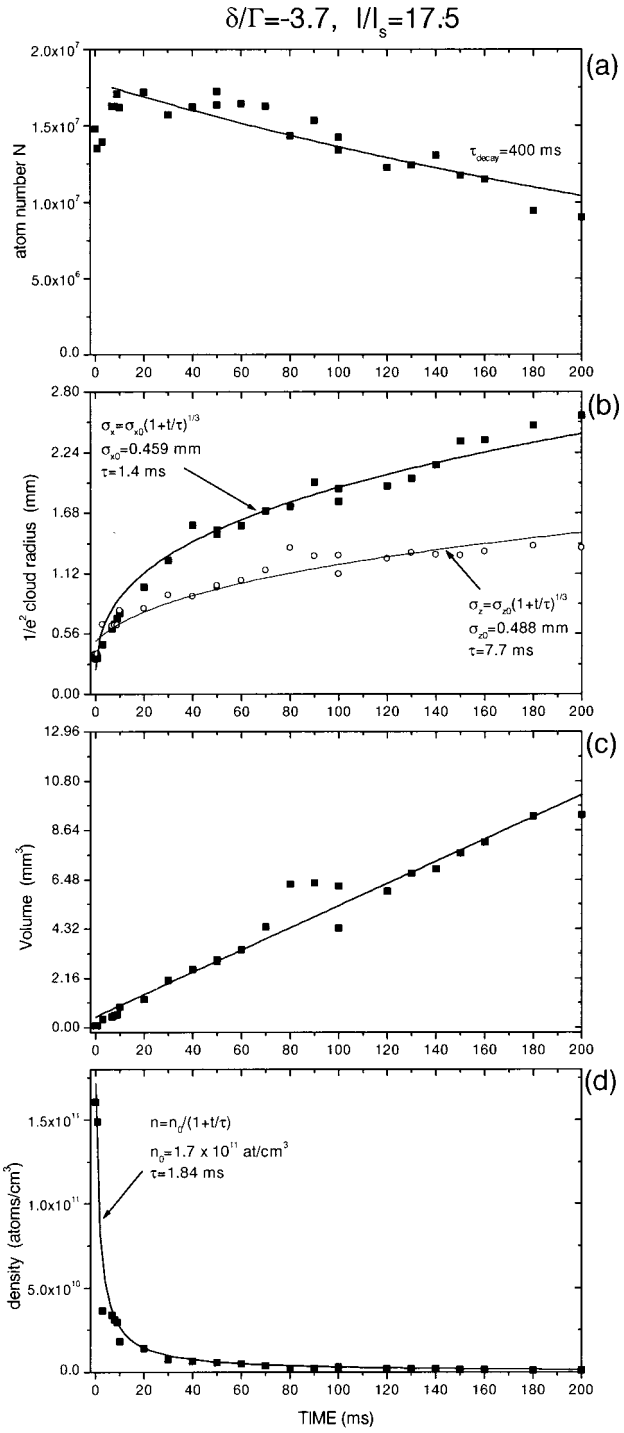

FIG. 3. Time evolution of the cloud: (a) the atom number and the fitted curve using an exponential decay function; (b) the cloud dimensions σ_x(■) and σ_z(○). Lines are the fitted curves with the function $\sigma=\sigma_0(1+t/\tau)^{1/3}$. (c) The cloud volume and the linear fitted curve. (d) The cloud density and the fitted curve using the function $n=n_0/(1+t/\tau)$.

We note that the experimental time scales for the expansion along the x axis and the z axis are somewhat different [Fig. 3(b)] with the characteristic time for the cloud expansion along the z axis being longer. This is due to the initial shape of the cloud in the MOT. Because of the anisotropy of the quadrupolar magnetic field, the cloud is not completely spherical.

The data analysis is performed in Sec. III D using the model of Coulomb explosion in a viscous medium. Details about the model are given in Secs. III B and III C.

B. Coulomb explosion in a viscous medium

The main ingredients of the model are the absorption, the radiation trapping and the friction forces. We will first present them explicitly and write the corresponding Fokker-Planck equation for the time evolution of the cloud. Then, the model will be applied to a spherical problem. The variation laws for the time evolutions of the volume and the density will be established in the case of a homogeneous sphere.

The expressions of the absorption force, $\vec{F}_A(\vec{r})$, and of the radiation trapping force, $\vec{F}_R(\vec{r})$, have been established by Dalibard [1] and Sesko, Walker, and Wieman [3]. Their space dependencies depend on the atomic density by the relation:

$$\vec{\nabla}\cdot[\vec{F}_A(\vec{r})]=-\sigma_L^2\frac{I}{c}n(\vec{r}), \tag{1a}$$

$$\vec{\nabla}\cdot[\vec{F}_R(\vec{r})]=\sigma_R\sigma_L\frac{I}{c}n(\vec{r}), \tag{1b}$$

where σ_L is the laser absorption cross section, σ_R is the absorption cross section of the scattered light, I is the laser light intensity, c is the light velocity, and $n(\vec{r})$ is the atomic density of the cloud. The expressions are valid in the linear regime for the light absorption (laser and the photons emitted by the atoms). Equation (1) are analogous to the well-known Maxwell equation and the Gauss' theorem can be used to derive the expression of the forces. The total force, $\vec{F}=\vec{F}_A+\vec{F}_R$, is then driven by

$$\vec{\nabla}\cdot[\vec{F}(\vec{r})]=Kn(\vec{r}) \tag{2}$$

where K is given by

$$K\equiv(\sigma_R-\sigma_L)\sigma_L I/c. \tag{3}$$

The coefficient K depends only on the laser intensity and frequency. Details about the calculation of σ_L, σ_R and K are given in the Appendix for the two-level atom. In most cases, σ_R is larger than σ_L and according to Eqs. (2) and (3), the force F expels the atoms out of the high-density region.

The friction force is assumed to be linearly dependent on the atom velocity $\vec{\nu}$ as

$$\vec{F}_f=-\alpha\vec{\nu}, \tag{4}$$

where α is the friction coefficient. Analytical or numerical calculations of α have been done in many laser configurations [16–19], mostly for linear $\perp$ linear polarizations of the lasers. For the $\sigma^+-\sigma^-$ configuration, in a low laser intensity regime, the results indicate dependence on the laser polariza-

tion and on the laser frequency [16–18]. For the sub-Doppler 'cooling regime and in the case of low-saturation parameter, these results indicate also that α depends neither on the position nor on the atom velocity. They show that for large laser detuning, the friction parameter α varies as $1/\delta$. The time scale corresponding to the damping of velocity, given by m/α, is in the microsecond range, which is shorter than the observed expansion time scale [Fig. 3(b)]. That lets us to assume that the atom velocity is rapidly damped.

The time evolution of the cloud is derived from the Fokker-Planck equation including the friction force and the total force. In our approach we neglect the momentum diffusion term [1,12,13]. With this assumption the Fokker-Planck equation for the normalized Wigner distribution $w(\vec{r},\vec{\nu},t)$ is:

$$\frac{\partial w(\vec{r},\vec{\nu},t)}{\partial t}+\vec{\nu}\cdot\vec{\nabla}[w(\vec{r},\vec{\nu},t)] = -\frac{1}{m}\vec{\nabla}_{\nu}\cdot\{[\vec{F}(\vec{r})+\vec{F}_f(\vec{\nu})]w(\vec{r},\vec{\nu},t)\} \times\int\int w(\vec{r},\vec{\nu},t)d^3\vec{r}d^3\vec{\nu}=1. \tag{5}$$

The atomic density, given by $n(\vec{r},t)=N\int w(\vec{r},\vec{\nu},t)d^3\vec{\nu}$ where N is the atom number, deduced from Eq. (5) by a velocity integration, is driven by

$$\frac{\partial n(\vec{r},t)}{\partial t}=-N\vec{\nabla}\cdot\left[\int\vec{\nu}w(\vec{r},\vec{\nu},t)d^3\vec{\nu}\right]. \tag{6}$$

Because of the rapid damping of the atom velocity, an adiabatic elimination of the velocity variables is possible [1]. The atom located at the position $\vec{r}$ rapidly reaches a limit velocity equal to $\vec{\nu}\approx\vec{F}(\vec{r})/\alpha$. Inserting this relation in the right-hand side of Eq. (6) results in the time evolution of the density:

$$\frac{\partial n(\vec{r},t)}{\partial t}=-\frac{1}{\alpha}\vec{\nabla}\cdot[\vec{F}(\vec{r})n(\vec{r},t)]. \tag{7}$$

Solving Eqs. (7) and (2) gives the time evolution of the cloud density. Because the position and velocity distributions are strongly correlated, the knowledge of the density determines velocity distribution and therefore the mean velocity (see Sec. IV).

C. Coulomb explosion in a spherical viscous medium

In order to illustrate the time evolution of the cloud density we will consider some spherical problems. First, we will give the solution for the Coulomb explosion in the case of an initially homogeneous sphere, and then for an initially gaussian shaped cloud.

Assuming spherical symmetry, the total force $\vec{F}$ is radial and the density depends only on the radial variable r, distance to the center of the cloud. Eq. (7) is thus expressed as

$$\frac{\partial n(r,t)}{\partial t}=-\frac{1}{\alpha}\frac{1}{r^2}\frac{\partial}{\partial r}[r^2F(r)n(r,t)]. \tag{8}$$

Equation (8), integrated by parts, allows to derive the evolution of the mean radius $\langle r\rangle=1/N\int rn(r)4\pi r^2dr$ in the form

$$\frac{\partial\langle r\rangle}{\partial t}=\frac{\langle F\rangle}{\alpha}, \tag{9}$$

where $\langle F\rangle$ is the mean force defined by $\langle F\rangle=1/N\int F(r)n(r,t)4\pi r^2dr$. Equation (9) relates the mean radial force $\langle F\rangle$ to the time evolution of the cloud size.

Now we assume that, at $t=0$, the cloud containing N atoms is a homogeneous sphere of radius R_0. Its initial density is then

$$n(r,t)=0=n_0=\frac{N}{4/3\pi R_0^3}\ \text{ for }\ r\leqslant R_0. \tag{10}$$

Equations (2) and (8) then imply that the spatial distribution stays spherically symmetric and homogeneous during the time evolution. The density at time t is then

$$n(r,t)=n(t)=\frac{N}{4/3\pi R(t)^3}\ \text{ for }\ r\leqslant R(t), \tag{11}$$

where $R(t)$ is the sphere radius at time t. A combination of Eqs. (2) and (8) leads to

$$\frac{\partial n(t)}{\partial t}=-\frac{K}{\alpha}n(t)^2, \tag{12}$$

which is solved

$$\frac{1}{n(t)}=\frac{1}{n_0}+\frac{K}{\alpha}t. \tag{13}$$

Equation (13) shows the linear time evolution of the inverse of the atomic density. The slope, K/α, depends only on the laser parameters and does not depend on the cloud parameters, e.g., the size or the atom number. Another form of Eq. (13) is $4\pi R(t)^3/3=4\pi R_0^3/3+KNt/\alpha$, which indicates a linear increase of the cloud volume versus time. The expansion rate KN/α is proportional to the cloud atom number and depends on the laser intensity and detuning via the ratio K/α. Introducing the time constant $\tau=\alpha/(Kn_0)$, the relative linear expansion of the cloud volume V and the reduction of its density n can be expressed by

$$V/V_0=1+t/\tau, \tag{14a}$$

$$n/n_0=(1+t/\tau)^{-1}, \tag{14b}$$

τ represents the time scale within the atomic cloud reaches twice its initial volume or half its initial density. The use of Eqs. (2) and (9) leads to the evolution of the mean radius $\langle r\rangle$ as

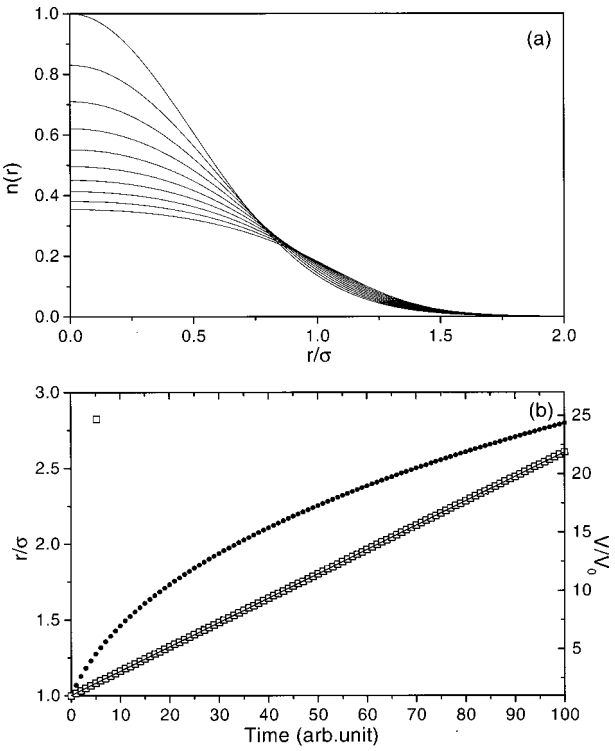

FIG. 4. Time evolution of the initially Gaussian shaped cloud: (a) spatial distribution of the atom in the cloud; (b) time evolution of the mean radius, $\overline{r}/\sigma$, (●), normalized to the initial size and of its cube $(\overline{r}/\sigma)^3$ (□) which varies linearly with time (fitted curve).

$$\langle r\rangle = \frac{3}{4}R(t) = \langle r_0\rangle(1+t/\tau)^{1/3}. \tag{15}$$

In order to improve our description of the experimental conditions, we have performed an analysis of the Fokker-Planck equation with an initially gaussian shaped cloud density. The cloud shape at $t=0$ is chosen as

$$n(r,t=0) = n_0(r) = \frac{N}{(\pi/2)^{3/2}\sigma^3}e^{-2r^2/\sigma^2}, \tag{16}$$

where σ is the $1/e^2$ radius of the distribution. The solution was performed numerically. As shown in Fig. 4(a), the cloud shape changes in time. The final shape is no longer a gaussian function. The knowledge of the density, $n(r,t)$, gives the mean radius, $\langle r\rangle$, of the cloud. The time evolution of $\langle r\rangle/\sigma$ is given in Fig. 4(b) simultaneously with the relative mean volume $(\langle r\rangle/\sigma)^3$. The results show a linear evolution in time for the mean volume. The time constant is equal to $\tau = 2.38\alpha/[Kn_0(r=0)]$ where $n_0(r=0)$ is the initial atomic density at the center of the cloud.

D. Experimental data analysis

The results of the previous section are used to fit the experimental data. The fitted curves are plotted in Fig. 3. With the experimental parameters, the cloud is not perfectly spherical, so we have introduced two time constants, one for the cloud evolution along the coil x axis and another along the z axis [Fig. 3(b)]. The data for V in Fig. 3(c) and for n in Fig. 3(d) are fitted for time less than 150 ms with the laws of Eq. (14). On this time scale, the atom number can be considered as constant. The latter condition is implicitly assumed in our model. The slope obtained from the linear fit in Fig. 3(c) is the expansion rate KN/α. With the measured atom number we deduce the ratio K/α. A fit of the density plot [Fig. 3(d)] by the Eq. (14b) gives another value of $K/\alpha(3.2\,10^{-15}\,\mathrm{m^3/s/atom})$ which differs from the previous one by only 10%.

In order to evaluate the quantity K/α, we have used a model based on the two-level atom interacting with an intense laser field to calculate K and the results of Ref. [16] to evaluate α. According to Eq. (3) an evaluation of K requires the knowledge of the absorption cross sections, σ_L for the laser light absorption, and σ_R for the scattering light reabsorption. All the details of the calculation are given in the Appendix. To calculate σ_R we have used the dressed atom approach [20], which leads to an analytical expression for σ_R. The calculation performed by Sesko, Walker, and Wieman [3] uses an exact expression for emission and absorption spectra, and takes into account the space modulation of the laser light in the trap but does not include a multi-level description of the atom. For $\delta/\Gamma=-3.7$, and $I/I_s=17.5$, calculations give $\sigma_L/\sigma_0=0.014$, $\sigma_R/\sigma_0=0.042$, and $K=8.33\,10^{-36}\,\mathrm{Nm^2/atom}$. A rigorous evaluation of α requires a 3D calculation of the cooling process in the case of large saturation parameters and a multilevel atom. To our knowledge only 1D or low-saturation cases have been treated for the $\sigma_+-\sigma_-$ configuration. Nevertheless, the results of Ref. [16] give a reasonable order of magnitude estimate for the friction parameter α. Formula (5.14) of Ref. [16] gives $\alpha=310^{-21}\,\mathrm{Ns/m}$. We thus get $K/\alpha=2.8\,10^{-15}\,\mathrm{m^3\,s^{-1}/atom}$, which is in good agreement with the measurement.

As mentioned above, the ratio K/α depends only on the laser characteristics (detuning and intensity). To check this property we have varied the cloud atom number, i.e., by changing the magnetic gradient of the magneto-optical trap. As shown in Fig. 5, the slope of the inverse density $1/n$ versus time is nearly independent of the initial atom number and initial density for magnetic field gradients in the range 11.5–21 Gauss/cm. Some discrepancies are observed for small magnetic gradients because the clouds are more dilute and larger.

Because coefficient K varies as $1/\delta^4$ at large laser detuning ($|\delta|\gg\Gamma$), (see the appendix) and the friction coefficient α varies as $1/|\delta|$, a variation of K/α as $1/|\delta|^3$ is expected. Figure 6 shows the time evolution of the density for a set of laser detunings. For $\delta/\Gamma=-1.5$, -3.7, -3.8 (not shown in the figure), -5.4 and -6.8 (not shown in the figure) the measurement of the K/α coefficient is in a good agreement with the prediction, either for the magnitude or for the scaling with the detuning. For a laser detuning $\delta/\Gamma=-2.5$ (circles in Fig. 6) the expansion rate is more than ten times lower than the expected value. With this detuning the number of trapped atoms is at the maximum (about 8.10^7 to 10^8 atoms). The small expansion rate can be explained neither by collision effects as suggested by Ref. [7] nor

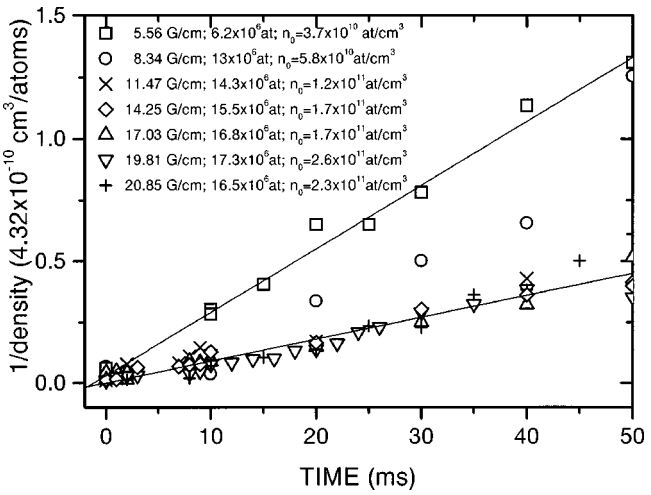

FIG. 5. Time evolution of the inverse of the density for different magnetic gradients.

by a nonlinearity of the friction force [12,16,18], because of the order of magnitude and of the sign of these effects. A possible explanation is a maximum value of the friction coefficient. The evaluation of the friction coefficient we have used assumes a cooling process in the low-saturation regime. In our case, the laser light is intense and the friction coefficient could be larger, as it has been observed in Ref. [21]. This study, concerning a one-dimensional cooling experiment using intense laser light, shows an increase of the capture and the friction coefficient. The explanation is based on coworking of the Doppler cooling and Sisyphus cooling.

IV. COOLING OF THE EXPANDING BRIGHT MOLASSES

In the case of spherical symmetry, because of the small velocity damping time, the radial velocity of the atom located at the position r is given by $v(r)=F(r)/\alpha$. Using Eq. (3) and Gauss's theorem for the homogeneous spherical cloud, the force is $F(r)=Knr/3$. The force varies linearly with the position variable, thus the velocity distribution is homogeneous. The maximum value of the radial velocity is

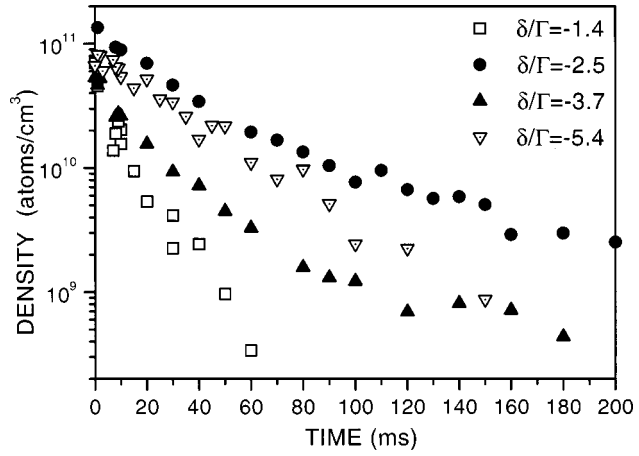

FIG. 6. Time evolution of the density for a set of laser detuning, for $I\sim 20I_S$. For $\delta/\Gamma=-2.5$, the expansion rate is very low.

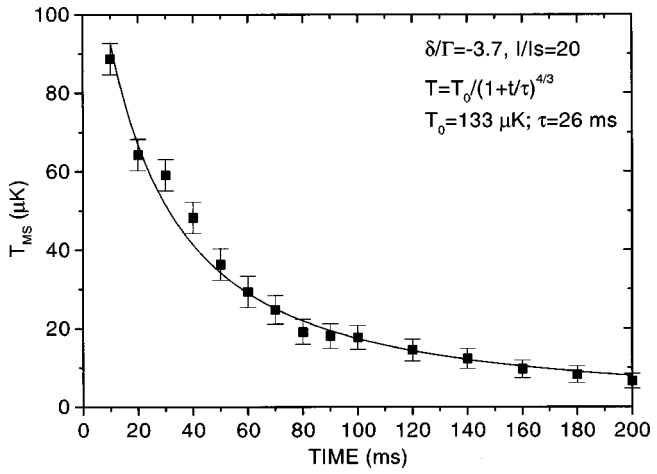

FIG. 7. Time evolution of the cloud temperature for $\delta/\Gamma=-3.7$, $I/I_S=20$ and the fitted data curve with the function $T_{\mathrm{MS}}=T_0/(1+t/\tau)^{4/3}$.

obtained at $r=R(t)$ and is equal to

$$\nu_M=\frac{K}{\alpha}\frac{N}{4\pi R(t)^2}. \tag{17}$$

The mean square velocity is therefore: $\langle \nu^2\rangle=3\nu_M^2/5$. Using the following definition of the temperature $k_BT_{\mathrm{MS}}=m\langle \nu^2\rangle$, Eqs. (16) and (14), we obtain the time evolution of the cloud temperature as $1/R(t)^4$ and

$$T_{\mathrm{MS}}=\frac{T_0}{(1+t/\tau)^{4/3}}, \tag{18}$$

where T_0 is the temperature at $t=0$, and τ is the time constant defined in the previous section. We note that the quantity $T_{\mathrm{MS}}V^{4/3}$ is constant during the cloud expansion.

The laws obtained for the cloud expansion and the temperature have to be restricted to the multiple scattering regime. The momentum diffusion has been neglected. The treatment is valid as the mean force $\langle F\rangle$ is larger than $D/R(t)$, where D is the spatial diffusion constant [1,12]. The condition can be expressed as

$$R(t)\ll\frac{3}{16\pi}\frac{KN}{\alpha D}. \tag{19}$$

In our experimental situations this condition is satisfied for clouds containing 10^7 atoms with radius less than a few millimeters.

Figure 7 shows T_{MS} obtained for $\delta/\Gamma=3.7$ and $I/I_s=20$, $N=3.5\,10^6$, and $n_0=1.4\,10^{10}$ atom/cm^3. The decrease of the temperature is observed as the cloud size increases. We check, by the temperature values, that the experiment is done in the sub-Doppler regime. The data curve is well fitted by Eq. (18), with $\tau=26$ ms and $T_0=133\,\mu$K. The corresponding evolution of the cloud density (not shown here) has been fitted by Eq. (14b) with a time constant equal to 15 ms.

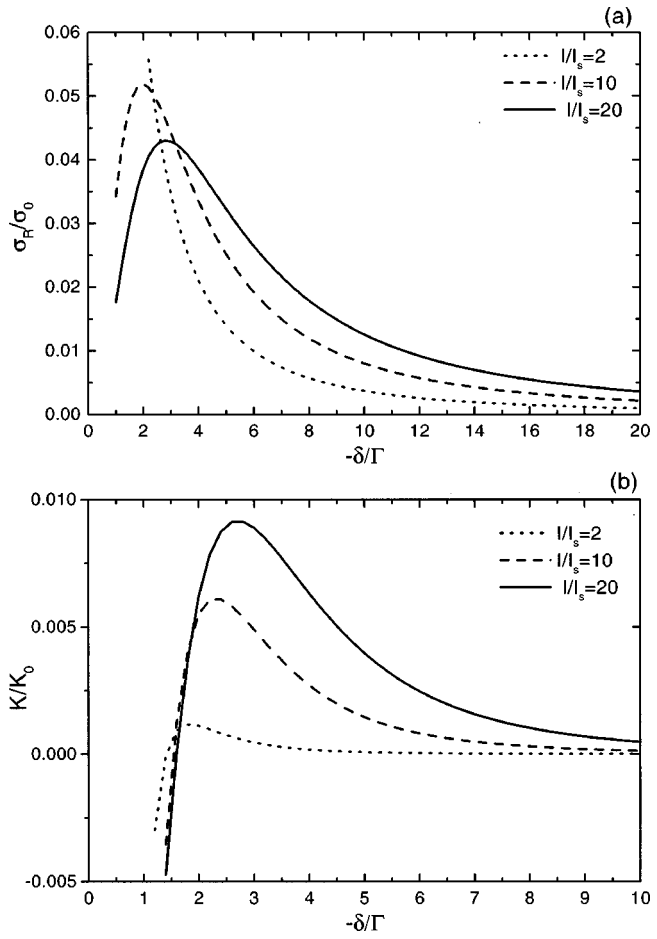

FIG. 8. Coefficients σ_R/σ_0 and K/K_0 with $K_0=\sigma_0^2 I_s/c$, versus the laser detuning (normalized to Γ), for a set of laser intensities. The plots are restricted to $\delta>1$ because of the validity of our model.

The obtained value of T_0 is in qualitative agreement with the predicted value using the maximum radial velocity given by Eq. (17).

We have verified that the quantity $T_{\mathrm{MS}}V^{4/3}$ is constant during the expansion of the cloud. This law characterizes the bright molasses expansion. Note that some other laws connecting the temperature, the volume and the atom number have already been demonstrated [22–24]. These studies only concern cases of large laser detunings and small laser intensities and do not examine the multiple scattering regime.

V. CONCLUSIONS

We have shown that the time evolution of an OM in the multiple scattering regime behaves as a Coulomb explosion in a viscous medium, because the radiation trapping force is analogous to the Coulomb law. The first main advantage of our system is the time scale, which is longer than in molecules, clusters or plasma, leading to easier observations. The second advantage is the possibility to change the ''charge'' of the Coulomb interaction by a change of the laser parameters. The third advantage is the possibility to study the Coulomb explosion without any other competitive processes.

With such a system, we have observed the expansion of the cloud. The phenomenon is characterized by a linear variation of the cloud volume in time. We have checked the variation of the time constant with the laser parameter, in particular with the laser detuning. Simultaneously to the expansion, the cloud is cooled down. The cooling process can be qualitatively understood by the escape of the ''blue'' photon out of the cloud. These photons, staying in the cloud, are responsible of the heating of the neighbor atoms. With these observations we can conclude that the expansion occurs with the conservation of the quantity $T_{\mathrm{MS}}V^{4/3}$.

ACKNOWLEDGMENTS

The authors express their appreciation for many useful comments and discussions with Christophe Blondel about this work. We also thank Anne Crubellier and Vladimir Akulin for useful discussions. Joshua Jortner expresses sincere thanks for the support of the International Chair 'Blaise Pascal' of the Fondation de l'Ecole Normale Supérieure.

APPENDIX

We present details of the calculation of absorption cross section σ_L, the reabsorption cross section σ_R and the coefficient K, in the case of the two-level atom, and using the dressed atom approach.

We consider a two-level atom illuminated by an intense quasi resonant monochromatic light. The absorption cross section is

$$\sigma_L=\frac{\sigma_0}{1+I/I_s+4\delta^2/\Gamma^2},$$

where σ_0 is the absorption cross-section at resonance, I is the laser intensity, I_s is the saturation intensity of the transition, δ is the laser light detuning and Γ is the natural width of the excited level. For the rubidium atom D_2 line, $\sigma_0=1.5\,10^{-9}\,\mathrm{cm}^2$, $I_s=1.62\,\mathrm{mW/cm}^2$, $\Gamma/2\pi=5.89\,\mathrm{MHz}$.

The reabsorption cross section is obtained by the evaluation of the absorption of the emitted light by the neighboring atoms. If $S(\omega)$ denotes the emission spectral density and $\sigma_A(\omega)$ the absorption spectra of the atom illuminated by the laser light, the re-absorption cross section is equal to

$$\sigma_R=\int \sigma_A(\omega)S(\omega)d\omega.$$

The fluorescence spectra, and the absorption spectra, are those of the atom in the presence of the intense laser light [4–6,20]. They can be expressed with the approach of Refs. [4–6] or by using the dressed atom approach [20]. In the dressed atom formalism, the normalized emission and absorption spectra are given by

$$S(\omega)=\frac{(c^2-s^2)^2}{c^4+s^4}L(\omega-\delta,0)+\frac{4c^4s^4}{c^4+s^4}L(\omega-\delta,\Gamma_p)\times c^2s^2\{L(\omega-\delta-\Omega_G,\Gamma_c)+L(\omega-\delta+\Omega_G,\Gamma_c)\}$$

and

$$\sigma_A(\omega)=\sigma_0\frac{\pi\Gamma}{2}\frac{c^2-s^2}{c^4+s^4}\times\{c^4L(\omega-\delta-\Omega_G,\Gamma_c)-s^4L(\omega-\delta+\Omega_G,\Gamma_c)\},$$

where $\Omega=\Gamma\sqrt{I/(2I_s)}$ is the Rabi frequency, $\Omega_G=\sqrt{\Omega^2+\delta^2}$ is the generalized Rabi frequency, $c^2=\cos^2(\theta)$, $s^2=\sin^2(\theta)$, $c^4=\cos^4(\theta)$, $s^4=\sin^4(\theta)$, with the angle θ defined by $\tan(2\theta)=\Omega/\delta$. The photon frequency ω is referenced to the atomic transition. $L(\omega-\omega',\Gamma')$ is the Lorentzian normalized function, centered at $\omega=\omega'$ with a width equal to 2Γ, and $L(\omega-\omega',0)$ its limit when Γ tends to zero, namely the delta function. Γ_p and Γ_c are given by

$$\Gamma_p=\Gamma(c^4+s^4)$$

and

$$\Gamma_c=\Gamma\frac{1+2c^2s^2}{2}.$$

These formula are valid if the generalized Rabi frequency is much larger than the natural width of the transition. In our case the condition is not fulfilled at small laser detuning and weak laser intensity.

The reabsorption cross section is then easily deduced and is equal to:

$$\sigma_R=\sigma_0\frac{\Gamma(c^2-s^2)^2}{2(c^4+s^4)}\left\{\frac{(c^2-s^2)^2}{c^4+s^4}\frac{\Gamma_c}{\Omega^2+\delta^2+\Gamma_c^2}+\frac{4c^4s^4}{c^4+s^4}\frac{(\Gamma_c+\Gamma_p)}{\Omega^2+\delta^2+(\Gamma_c+\Gamma_p)^2}+\frac{c^2s^2}{2}\times\left(\frac{1}{\Gamma_c}+\frac{\Gamma_c}{\Omega^2+\delta^2+\Gamma_c^2}\right)\right\}.$$

The coefficient K is given by $K=(\sigma_R-\sigma_L)\sigma_L I/c$. Plots of σ_R and K, versus the laser detuning are given in Fig. 8, for a set of laser intensities. Calculations done with the Mollow's approach [4–6] give the same results for large values of laser detuning and for large intensities. Discrepancies are observed for very small laser detunings ($|\delta|<\Gamma$) which is achieved our experiments.

Asymptotic laws for previous formula are given. For large laser detuning, $|\delta|\gg\Omega\gg\Gamma$ one gets $\theta\approx\Omega/(2\delta)$ and the previous relations give

$$\sigma_L\approx\sigma_0\frac{\Gamma^2}{4\delta^2},\quad \sigma_R-\sigma_L\approx\sigma_0\frac{\Omega^2}{8\delta^2},\quad \text{and}\quad K\approx\frac{\sigma_0^2I_s}{c}\frac{\Omega^4}{16\delta^4}.$$

The other limit is obtained for large laser intensity $\Omega\gg\delta\gg\Gamma$. In this case, one has $\cos(2\theta)\approx\delta/\Omega$ and $\sin(2\theta)\approx1-\delta^2/(2\Omega^2)$ and a Taylor's expansion leads to

$$\sigma_L\approx\sigma_0\frac{\Gamma^2}{2\Omega^2},\quad \sigma_R-\sigma_L\approx\sigma_0\frac{\delta^2}{6\Omega^2},\quad \text{and}\quad K\approx\frac{\sigma_0^2I_s}{c}\frac{\delta^2}{6\Omega^2}.$$

[1] J. Dalibard, Opt. Commun. **68**, 203 (1988).
[2] T. Walker, D. Sesko, and C. Wieman, Phys. Rev. Lett. **64**, 408 (1990).
[3] D. W. Sesko, T. G. Walker, and C. E. Wieman, J. Opt. Soc. Am. B **8**, 946 (1991).
[4] B. R. Mollow, Phys. Rev. **188**, 1969 (1969).
[5] R. E. Grove, F. Y. Wu, and S. Ezekiel, Phys. Rev. A **15**, 227 (1977).
[6] F. Y. Wu, S. Ezekiel, M. Ducloy, and B. R. Mollow, Phys. Rev. Lett. **38**, 1077 (1977).
[7] A. M. Steane, M. Chowdbury, and C. J. Foot, J. Opt. Soc. Am. B **9**, 2142 (1992).
[8] W. Petrich, M. H. Anderson, J. R. Ensher, and E. A. Cornell, J. Opt. Soc. Am. B **11**, 1332 (1994).
[9] M. Drewsen, P. Laurent, A. Nadir, G. Santarelli, A. Clairon, Y. Castin, D. Grison, and C. Salomon, Appl. Phys. B: Lasers Opt. **B59**, 283 (1994).
[10] V. S. Bagnato, L. G. Marcassa, M. Oria, G. I. Surdutovich, R. Vitlina, and S. C. Zilio, Phys. Rev. A **48**, 3771 (1993).
[11] D. Boiron, A. Michaud, P. Lemonde, Y. Castin, C. Salomon, S. Weyers, K. Szymaniec, L. Cognet, and A. Clairon, Phys. Rev. A **53**, R3734 (1996).
[12] T. W. Hodapp, C. Gerz, C. Furtlehner, C. I. Westbrook, W. D. Phillips, and J. Dalibard, Appl. Phys. B: Lasers Opt. **60**, 135 (1995).
[13] A. G. Truscott, D. Baleva, N. R. Heckenberg, and H. Rubinsztein-Dunlop, Opt. Commun. **145**, 81 (1998).
[14] K. Boyer, T. S. Iuk, J. C. Solem, and C. K. Rhodes, Phys. Rev. A **39**, 1186 (1989).
[15] I. Last, I. Scheck, and J. Jortner, J. Chem. Phys. **107**, 6685 (1997).
[16] J. Dalibard and C. Cohen-Tannoudji, J. Opt. Soc. Am. B **6**, 2023 (1989).
[17] K. Molmer, Phys. Rev. A **44**, 5820 (1991).
[18] A. M. Steane, G. Hillenbrand, and C. J. Foot, J. Phys. B **25**, 4721 (1992).
[19] I. Javanainen, J. Phys. B **27**, L41 (1994), and references therein.
[20] C. Cohen-Tannoudji, *Cargese Lectures in Physics*, edited by M. Levy (Gordon and Breach, New York, 1968); C. Cohen-Tannoudji, J. Dupont-Roc, and G. Grynberg, *Processus d'Interaction entre Photons et Atomes* (Inter Editions et Edition du CNRS, Paris, 1988).
[21] M. R. Williams, M. J. Bellanca, L. Liu, C. Xie, W. F. Buell, T. H. Bergeman, and H. J. Metcalf, Phys. Rev. A **57**, 401 (1998).
[22] D. Boiron, C. Triché, D. R. Meacher, P. Verkerk, and G. Grynberg, Phys. Rev. A **52**, R3425 (1995).
[23] A. Hemmerich, M. Weidemüller, T. Esslinger, C. Zimmermann, and T. Hänsch, Phys. Rev. Lett. **75**, 37 (1995).
[24] E Arimondo (private communication).